Test and Verification of Vortex Shedding for a 3D Bluff Body

Paul D Innes[1] and Charles E Carlson[2]
California Polytechnic State University,1 Grand Avenue, San Luis Obispo, CA, 93405

Testing of a 3D bluff body with and without end plate tabs was performed in the California Polytechnic State University 3x4 ft low speed wind tunnel. The C_P values were obtained for the test case with no end plate tabs for speeds of 10, 15, 20, and 30 m/s. It was observed that stronger vortex shedding ocured at the higher speed test cases. The model was shimmed to be at approximately 5° angle of attack in order to obtain symmetrical negative C_P spikes for the top and bottom of the model without tabs. Trends were observed and compared to trends previously noted in Jarred Pinn's thesis. The baseplate was replaced with one that contained tabs along the spanwise direction, and it was observed that the vortex shedding was eliminated with the addition of the base plate tabs. The data obtained confirmed previous trends seen that tabs resulted in reduced drag and elimination of vortex shedding at the top and bottom of the model base.

Nomenclature

AoA	=	angle of attack
C_p	=	pressure coefficient
p_∞	=	freestream static pressure
p_T	=	total stagnation pressure
q_∞	=	dynamic pressure
V	=	velocity
V_∞	=	freestream velocity

I. Introduction

THE study of bluff body objects is becoming an area of research that has many practical applications in an everyday environment including but not limited to large buildings, tractor trailers, and larger fixed and rotor wing aircraft. Understanding the flow along the body and at departure of the flow at the trailing edge of the body can help identify more effective and efficient integrations in the aforementioned to further improve the operating qualities. The commonality in the various bluff body objects is the large base regions which the different geometries inheritantly create. The trailing edge, flat base region that is perpendicular to the flow on these blunt bodies in prone to creating an area of separation and thus a low base pressure. The low base pressure on the bluff bodies can be attributed to an increase in drag seen by the object. The use of an interchangeable back plate is implemented to switch between a backplate that sits flush with the sides of the body and that of a backplate that has six tabs that protrude out the side. By further studying the characteristics surrounding the bluff body and the passive flow control techniques implemented, small improvements on drag can be identified and integrated into common transport bodies that could lead to a favorable change in the operating cost of a given body.

This project is a follow-up to the studies done by Jarred Pinn and Dr. Jin Tso to further verify the results obtained. The use of the same bluff body as that of Pinn in the Cal Poly Low-Speed Wind Tunnel should produce similar results as only interior aspects to the model were altered. The changes made to the model occur internally and concern the connections of the pressure ports to the tubing. Prior to running the experiments, it was determined that the safety wire previously used in the attachment of the tube to the pressure port was causing unnecessary wear and creating small holes in which error was introduced into the data. Furthermore, the use of COTS nail polish was used as an inexpensive and reliable replacement to the epoxy sealant used by Pinn.

[1] Undergradute Student, Aerospace Engineering, 1 Grand Ave, California Polytechnic State University, 93045
[2] Undergradute Student, Aerospace Engineering, 1 Grand Ave, California Polytechnic State University, 93045

II. Apparatus

The test model used in this experiment is a three dimensional bluff body constructed of 6061-T6 aluminum. The model was previously fabricated in the Cal Poly machine shop for use in Pinn's experiment on the "Effect of End – Plate tabs on Drag Reduction of a 3D Bluff Body with a Blunt Base." The components of the model consist of two 0.25 inch thick plates of aluminum for the sides and a 0.25 inch thick half cylinder piece of

Figure 1: The 3D Bluff Body with a Blunt Edge Model Used

aluminum for the leading edge. The model as a whole has geometric configuration such that the sides have a length of 12 inches, a width of 9.5 inches, and a base region depth of 2.38 inches, as shown in figure 1. The model is instrumented with a variety of pressure ports that span the depth of the leading edge, down the side of the model,

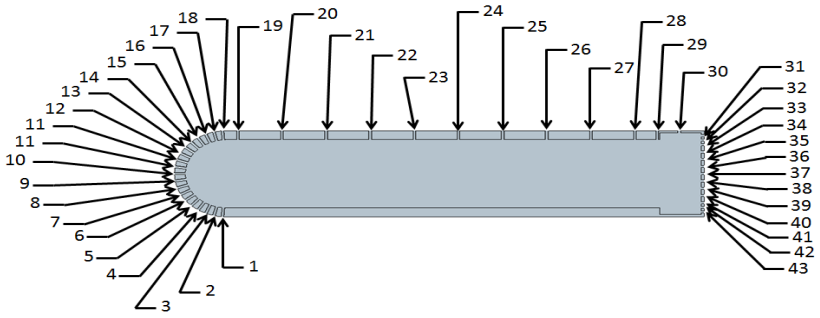

Figure 2: Location and numbering of the pressure ports instumented on the model

and in locations on the back plate as can be seen in figure 2. The rear plate of the model that has no tabs and sits flush with the rest of the body contains ports in both the spanwise and vertical directions. The 15 horizontal spanwise pressure ports shown in figure 3 are spaced 0.5 inches apart with exception to the two ports on either side of the centerline that are offset due to structural components of the model. To help minimize the imperfections within the surface and manufacturing process, a 1 inch 3M anti-slip tape model 7551N was added to the location just beyond the curvature of the leading edge as shown in figure 4. The second interchangeable back plate for the model is geometrically similar to the first but with the addition of overhanging tabs that protrude into the airflow by 0.1875 inches and have a width of 0.475 inches. The tabs, which are spaced 4 inches apart can be seen in figure 5. Modeling the first plate, pressure ports were of the same configuration with the addition of another vertical row of ports spaced in between two of the tabs as seen in figure5.

Figure 3: Spanwise pressure ports on backplate with no tabs.

Figure 4: Rough strips used at leading edge.

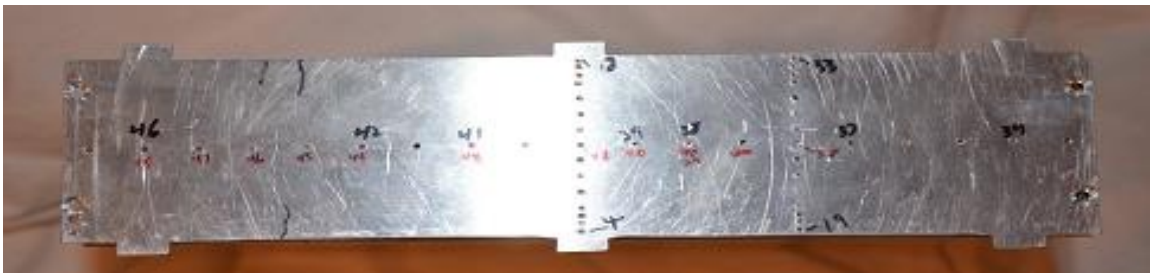

Figure 5: Spanwise pressure ports on backplate with tabs.

The tubes were connected to the pressure ports using nail polish which acted as a sealant to the port and an adhesive to the tubes. The nail polish provided an easy way to seal the tubing connections while not having to use safety wire in areas with geometrically tight constraints. The nail polish is easily removable, unlike the epoxy previously used, which will allow for easy interchange of hardware if needed. The nail polish was placed around the previously existing epoxied ports in some cases, but it proved to be strong enough to be used alone as a means to seal the tube and port interface. Figure 6 depicts the type and location of the nail polished used for the experiment. This solution was extremely cheap when compared to traditional epoxy or safety wire solutions, and it will most likely be implemented in future experiments due to its success. The safety wire connections on the tabbed model did

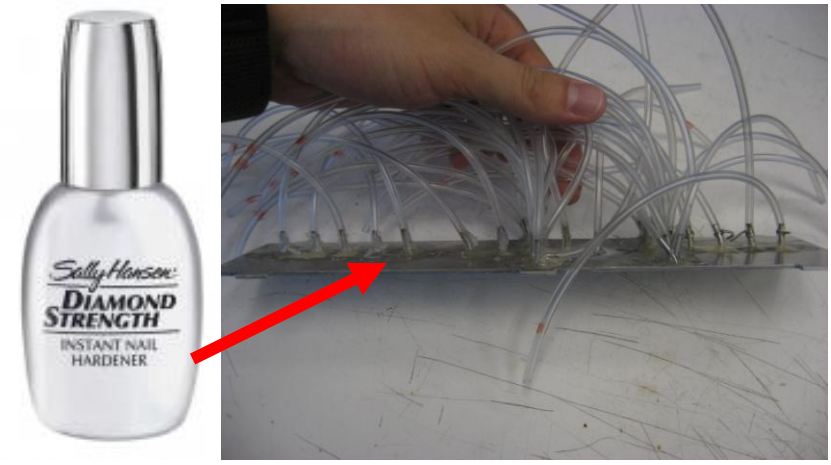

Figure 6: Nail Polish and locaion where nail polish was applied to port/tube interface.

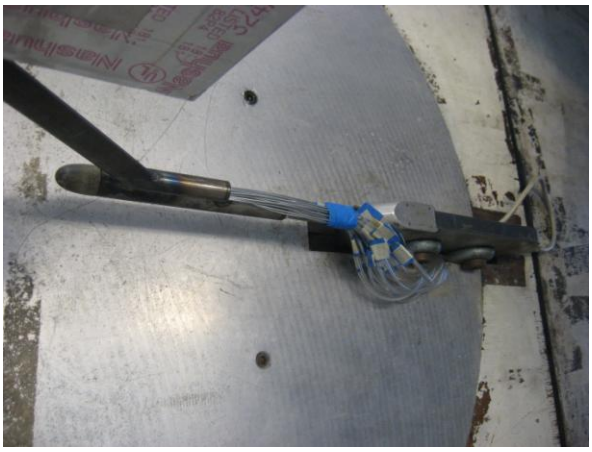

Figure 7: Pressure tubes routed into sting balance mount to the scannivalve.

not have to be replaced with the nail polish as they showed no pressure leaks when tested prior to being mounted on the back of the model. Tubes were then routed out of the model via an access port in the bottom and through the mounting strut as can be seen in figure 7.

The tubes were pressure tested via use of a handheld pressure pump in the form of a blood pressure as seen in the leftmost picture in figure 8. This pump was used to make sure that the pressure ports could hold pressure without leaking, which is indicated by the picture on the right in figure 8. After routing the tubes out of the wind tunnel, the loose ends are connected to a leak proof adapter plate that downsizes the tubing from 0.125 inches to 0.0313 inches with the smaller tubing being connected to the Scanivalve unit. A Scanivalve Z0C33/64x-X1 pressure scanner is used to measure the respective pressure in each port hooked up. The Z0C33 unit has the ability to support up to 64 pressure inputs and operates with a regulated 65 psi input to a pneumatic solenoid that switches the ports internally. Only 17 ports were used for this experiment as there were 15 ports on the model and freestream and stagnation pressures were taken upstream from the tunnel, making 17 measurements total. The boundary layer grows along the length of the tunnel, so the apparent speeds in the test section are higher at the test section than at the inlet of the tunnel. A pitot/static tube was used to measure local static and stagnation pressures where the model was

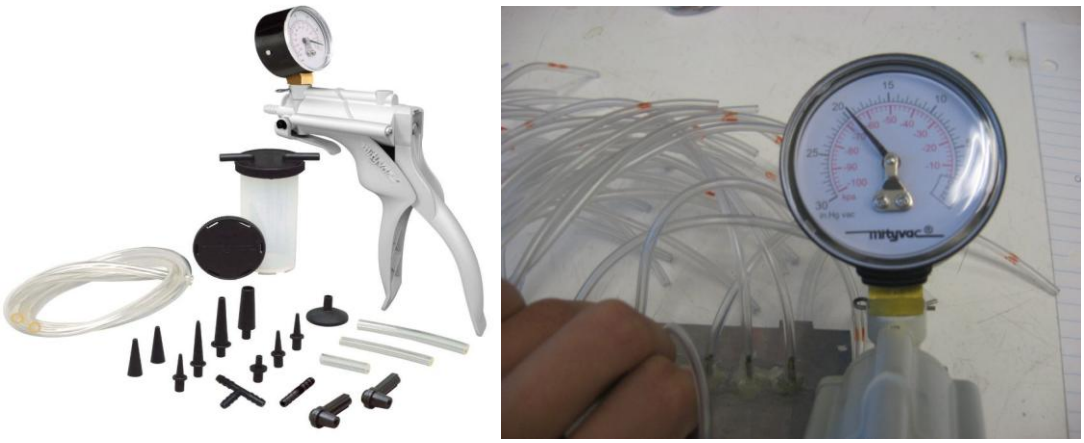

Figure 8: Handheld pressure pump (left) and pressure holding test for ports (right).

mounted, and it was placed approximately 7.5 inches from the wall of the tunnel. It is assumed that this places the probe well out of the boundary layer of the flow.

A Scanivalve RAD3200 analog-to-digital amplifier samples the +/- 2.5 Vdc output and amplifies the signal followed sending it through a USB Extender 3200 to a computer. RAD software V2.10 runs on the computer to connect the Z0C33 system and allows the Radlink software to operate. Radlink controls the system and allows the user to select which ports are to be recorded and at what rate.

The wind tunnel used in the experiment was the Cal Poly low speed wind tunnel as seen in figure 9. It is an open circuit wind tunnel that draws air through a straightening section containing a fine mesh followed by a plastic honeycomb. The flow then passes through a 10:1 duct section. The wind tunnel test section is comprised of multiple 3 x 4 foot removable sections and can range from 7 to 19 feet. This experiment was conducted in the last section which houses the sting balance and is the only non removable section. Flow is drawn through the tunnel by a belt driven 150 horsepower 440 volt three phase motor that turns a 9 bladed fixed pitch fan. The speed range used for testing in the tunnel is approximately 0 to 30 m/s.

Figure 9: Calpoly low speed wind tunnel used for the experiment.

III. Procedure

After properly assembling the model, it was mounted to the sting balance by the connecting strut. Prior to tightening the strut down, a level was used to verify that the model was plum the wind tunnel. After routing the pressure tubes out of the tunnel and hooking them up to the adapter plate, the Scanivalve is then operated through

the connections with the pressure tubing and the computer controller. The Scanivalve z0c33 uses a regulated air pressure of 65 PSI to operate the internal port switching that sequentially samples the 64 ports. The external pressure source was hooked to a designated port on the unit and steadily supplied by an in house system provided within the lab.

Using the software program Radlink, the Scanivalve unit was readily controlled through the computer. To run a test, one must first create a new data log to import the incoming data into. After picking the scan group of conFig.d, the ports being used are selected out of the 64 total pressure ports. The period is set to 50 microseconds and the average is set to 1, implying one scan per frame. Setting the frames per scan to 15,000 allows each pressure to be read for 50 microseconds 15,000 times. Yhe zero calibrate operation is run before each reading which essentially calculates the offset in the A/D between the measured zero and the data from when the last zero calibration was completed.

Before testing can be conducted, it is necessary to calibrate the flow through the wind tunnel. The calibration testing consists of comparing the static pressure measured after the converging section of the tunnel with the measured static pressure at the models location. A pitot static probe was used to measure the static and stagnation pressures of the flow near the model test section, and these values were used for calculation of C_P for the test days as it cannot be assumed that the inlet static and stagnation pressures are equal to test section static and stagnation pressures. As mentioned before, the inlet and test section pressures were measured using a pitot/static probe mounted 7.5 inches from the wall of the tunnel in the test section. The pitot/static probe was mounted with extreme care to ensure that the flow was parallel to the tube so that accurate stagnation pressures could be measured. The measurements were taken very close to the midpoint of the model strut mount and the wall of the test section in order to stay clear of the boundary layer and to accurately measure the flow that is approximately equal to the flow that the model sees when it is on the strut mount.

Once flow characteristics and measurement tool were properly calibrated, testing can be initiated on the rear plates. The rear plate that sits flush with the model geometry and has no tabs was used and tested. All the connections were checked and then sealed internally before the model was assembled in a secure fashion. Aluminum tape was used to seal the model to ensure that no leaking occurred while the tests were being run.The model was then mounted to the sting balance and shimmed as needed in order to guarantee alignment with the flow. Test were conducted at 10, 15, 20, and 30 m/s velocities. Pressure values were then recorded via use of the Scanivalve and transferred to the computer. Following testing on the plate that sits flush on the model, the tabbed plate was then installed in a similar fashion as that of the first plate and tests were run in an identical manor. The tabbed plate was used in order to estimate the drag reduction of the passive flow control via tabs.

IV. Analysis

In order to analyze pressure data obtained through experimental testing, the following equations were used in order to represent the data in terms of pressure coefficient and dynamic pressure. The Scannivalve software outputs the data in terms of pressures in units of psi, and this can then be converted to C_P if the free stream static and stagnation pressures are known. Bernoulli's equation can be manipulated to obtain an expression for the dynamic pressure, and this is represented by equation 1.

$$p_T - p_\infty = \tfrac{1}{2} \rho_\infty V_\infty^2 \quad \textbf{(1)}$$

The above statement can be re-written to show that the dynamic pressure is just the difference between the respective pressure and the free stream static pressure. The dynamic pressure used for calculations of C_P corresponds to the values taken in the test section of the tunnel, as opposed to the inlet. This simplified equation 2 can be used to find the dynamic pressure for each respective test point.

$$p_T - p_\infty = q_\infty \quad \textbf{(2)}$$

This value for dynamic pressure can be used to find the pressure coefficient at each respective port at the different flow speeds. Equation 3 shows the equation that was used to calculate pressure coefficient.

$$C_P = (p - p_\infty) / q_\infty \quad \textbf{(3)}$$

The pressure coefficient was plotted with respect to port location to observe negative spikes that are indicative of vortex shedding. The value of C_P is unitless, and is presented as such. All pressures were measured in psid, and velocities are represented in m/s.

V. Results and Discussion

The testing of the bluff body with a blunt base was performed to evaluate the effect of end-plate tabs in their ability to eliminate vortex shedding at the base. This vortex shedding suppression has the effect of reducing drag on the body which is desired for aerodynamic effectiveness. The data obtained was compared to previously taken data that showed vortex shedding suppression and end plate tab effectiveness which was performed by Jarred Pinn as part of his thesis on the "effect of end-plate tabs on drag reduction of a 3D bluff body with a blunt base." The results of the test as well as a comparison to previous data is discussed below.

A. Symmetrical C_P spikes for model with no-tabs

The first test of the model was performed in the no-tabs configuration of the base, and the pressures were measured across the spanwise direction of the model. The pressure ports are placed 0.5 inches apart, and a Scannivalve was used to take pressure measurements for each successive wind tunnel speed. The variation of pressure coefficients across the spanwise base can be seen in figure 10.

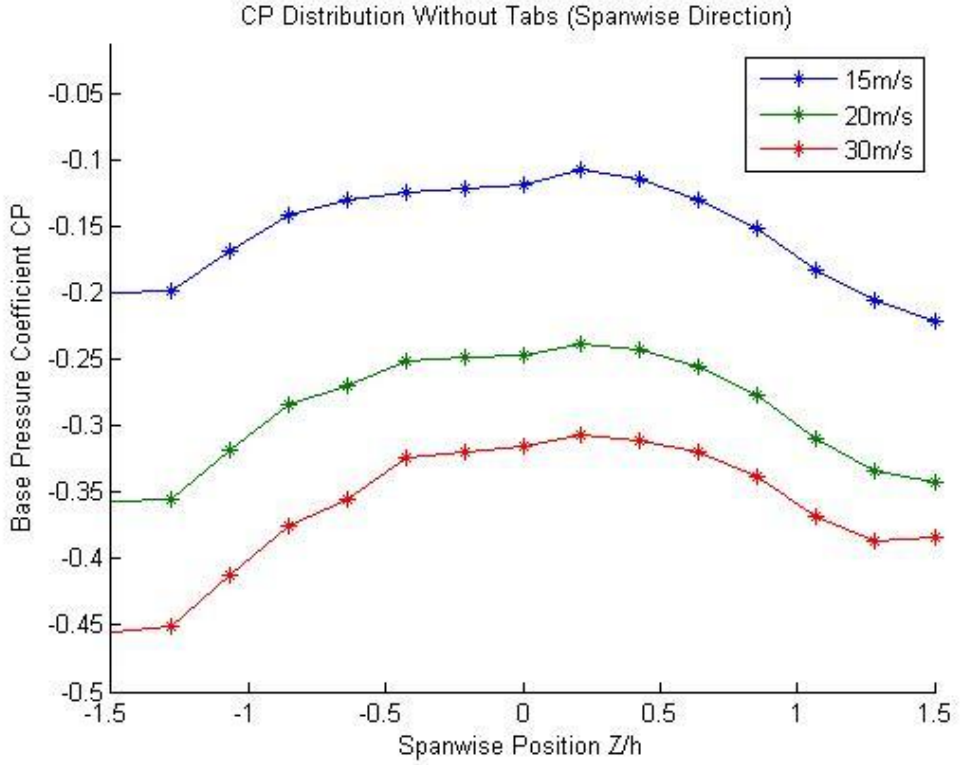

Figure 10: Spanwise base C_P distribution for model base without tabs for calibrated airspeeds. The model was shimmed to about 5° angle of attack.

The configuration without tabs showed negative C_P spikes at the top and bottom of the model base. It was extremely difficult to obtain symmetric C_P spikes for the top and bottom of the model because of the asymmetry of the bottom having a mounting strut. The C_P spikes were found to be at approximately -0.46 for the bottom of the model (Z/h=-1.5) and approximately -0.38 for the top of the model base (Z/h=1.5) at 30 m/s. The C_P spikes were found to be at approximately -0.36 for the bottom of the model and approximately -0.35 for the top of the model base at 20 m/s, and the C_P spikes were at approximately -0.2 for the bottom and approximately -0.22 for the top of the model base at 15 m/s. A somewhat stagnant C_P condition can be seen for the center section of the model, and this is indicative of fully separated flow. The negative spikes at top and bottom are indicative of vortex shedding at the top and bottom of the model, which was expected for the test configuration. The C_P values attained in figure 10 are calibrated for the flows static and stagnation pressures at the test section of the tunnel. The pitot/static measurements were used to calculate appropriate dynamic pressures that were representative of the actual speeds that were seen by the model. The calculated dynamic pressures for 15, 20, and 30 m/s contained an error of 1.5%, 2.1%, and 1.2% respectively for these speeds. The data was adjusted using these pressures taken at the test section instead of using

the initially measured static and stagnation of the inlet of the tunnel.The growing boundary layer was taken into account, and faster flow speeds exist farther down the tunnel than at the inlet. Multiple tests were performed without tabs at the base to get a symmetric result, and the model was shimmed at the strut mount location to approximately 5° angle of attack in order to get the results observed in figure 10.

The model was shimmed in successive increments while tests were run to try and achieve symmetry for the C_P spikes. A figure of the initial shimmed case can be seen in figure 11. This shows the trend that the model had to be shimmed to higher angles of attack in order for the vortex shedding at the top of the model to become very apparent. This plot was used to show trends of C_P, and the dynamic pressures used were from the tunnel inlet as the test section pressures had not been measured and implemented yet into the calculations. Figure 11 was not used to compare with other data, but it was purely used as a means to spot the trend that inclining the model with respect to freestream produced more favorable results. The pressure port at location 7 was found to be faulty for the case with no tabs, and this was observed and noted in previous testing done by Pinn. The ports on either adjacent sides of the defective port were averaged to create a continuous data set. This average is pictured in the plots for the purposes of this report. The pressures for the tabbed C_P case showed no discontinuous data at port 7, so it was assumed that all connections from the model to the scannivalve were free of leaks. It was investigated further after the model was disassembled, and it was found that pressure port 7 was completely clogged and no air could pass through the port. The port held pressure without the port being manually plugged when it was checked with the pressure pump, and this indicated that it had been clogged. The pressure port will have to be completely replaced if further experimentation of the model is to be pursued.

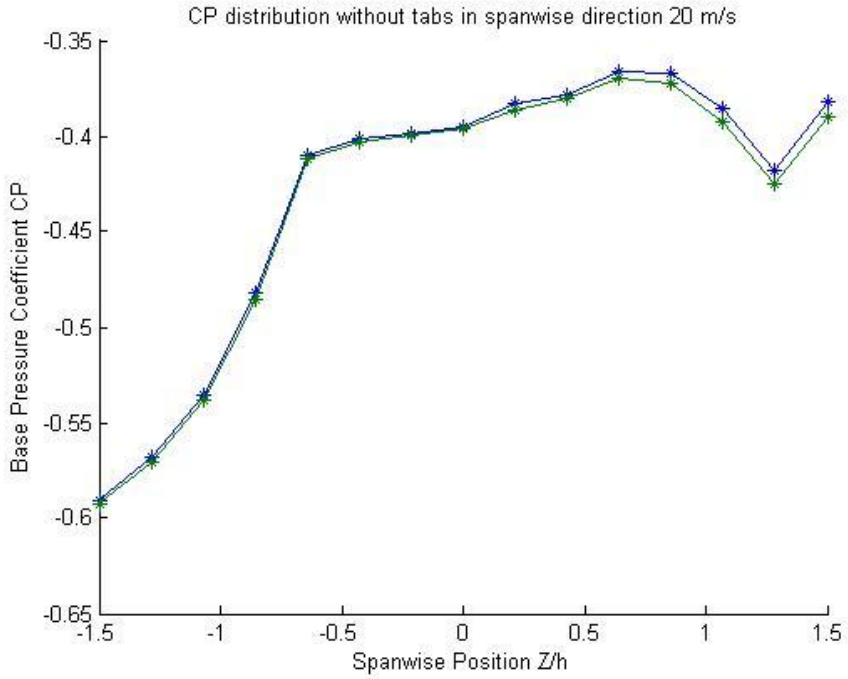

Figure 11: Spanwise base C_P distribution for model base without tabs after initia shim was perfomed at the strut interface location.

It can easily be seen in figure 11 that the vortex shedding at the top of the model is only slightly apparent and not symmetric in C_P with the bottom of the base. This test case was used to confirm the trend that the model would have to be inclined at a higher angle of attack in order to achieve the desired symmetric C_P spikes for the different speeds. The model was inclined to 5° angle of attack in order to get equal magnitudes for both top and bottom of the model. The model was put at higher angles of attack as it was decided that going past the 5° would be slightly unreasonable when comparing to the data obtained in previous tests by Jarred Pinn where the model was oriented at 0° angle of attack and no shimming was used. The model in the most shimmed case can be seen in figure 12, and there is visual confirmation that the model is tilted at a slightly positive angle of attack. The bottom of the model was streamlined with aluminum tape to ensure that the shimming has minimal effect on disturning the flow at the base of the model near the strut mount.

Figure 12: Model is shimmed at strut mount interface and streamlined with aluminum tape.

B. Vortex intensity trends

After the vortex shedding indications were achieved, the data was examined in order to try and see trends for vortex shedding intensity at different test speeds. The model was run with speeds of 15, 20, and 30 m/s in order to see any resulting trends of C_P spike magnitudes. The data obtained by Jarred Pinn in his thesis indicate that the vortex shedding is stronger for lower speeds, and the tests performed were in effect trying to confirm this observation. It was believed that the vortex shedding would be stronger for higher speeds as the air has more momentum and the pressure differences would be larger due to this increased speed of the flow. A comparison of the data obtained in the results of this experiment can be seen pictured below in figure 13 with Jarred's data obtained in previous testing as seen on the right.

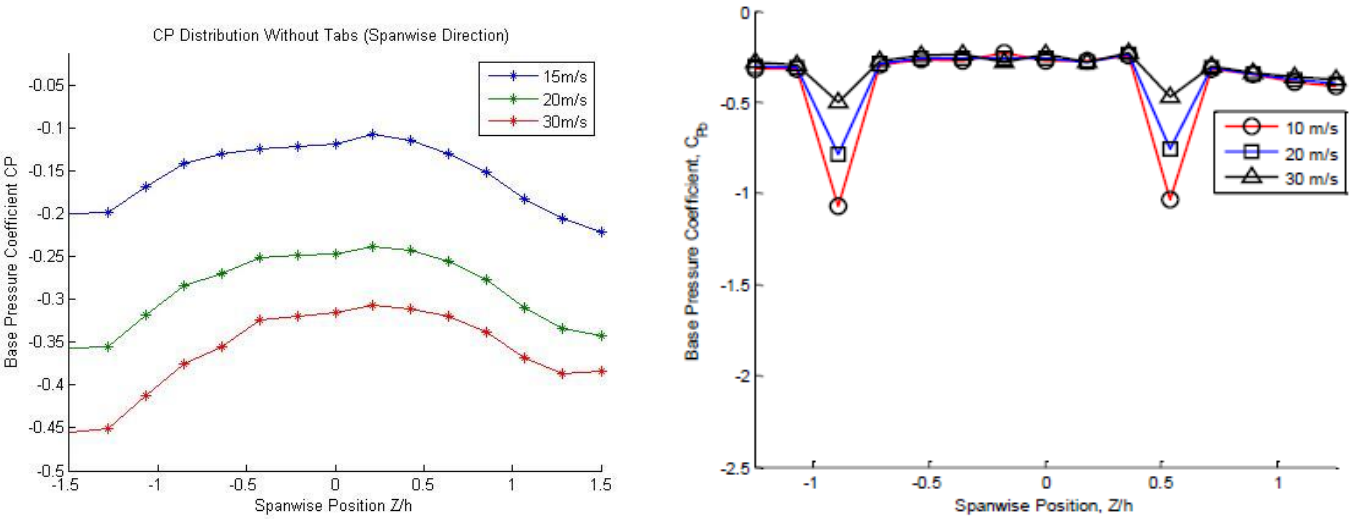

Figure 13: C_P spike trends seen in this experiment compared to previously obtained data.

It can be seen that the trends exhibited by the plot on the left in figure 13 indicate that the strength of vortex is stronger, higher C_P, at higher speeds. The 30m/s spike was at approximately -0.46, while the spike for the 10m/s case was around -0.2. The plot on the right indicates the opposite trend as the spike for the 30m/s case occurs at -0.5, and the spike for the slower 10m/s case is around -1.1. The test data produced by this experiment confirm that the

trends seen previously are different as it was expected that the vortex shedding would be greater at higher speeds. This can be seen by looking at the data in the plot on the left. The pressure differences should be greater at the base for higher speeds, and this is confirmed by the test results for differing speeds up to 30m/s. The asymmetry of the C_P spikes may be a factor of the strut mounted at the bottom of the model.

C. Test case with tabs

The end plate was removed and replaced with a plate that has tabs for passive drag reduction. The model was repositioned on the sting to be at 0° angle of attack, and the test was performed for speeds of 10, 20, and 30 m/s. It was expected that the addition of the tabs would eliminate the negative spikes of pressure coefficient for the base of the model. The trends exhibited by the model with tabs can be seen in figure 14.

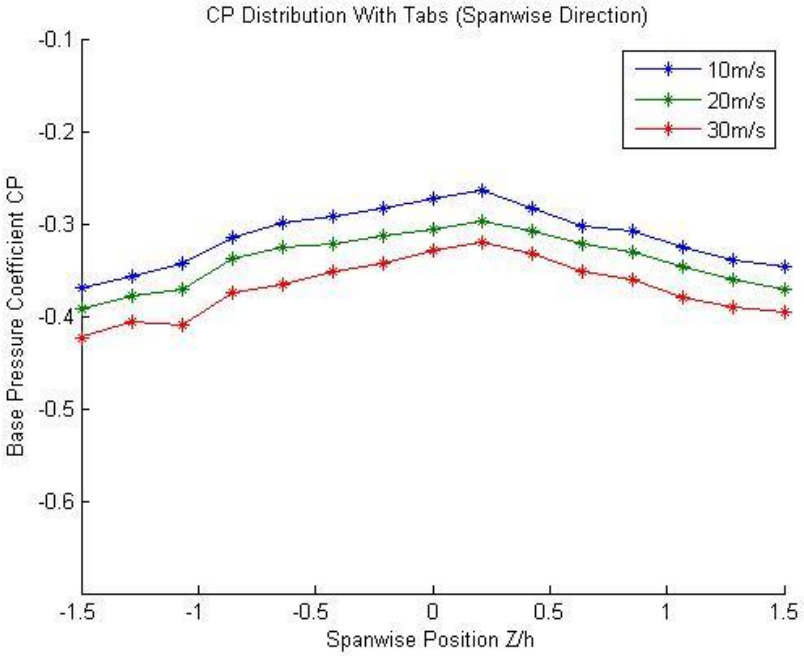

Figure 14: The base with tabs was used to show passive drag reduction.

The tabs produced trends with relatively flat C_P values. The negative spikes seen in the case with no tabs are eliminated in this test case, and the elimination of vortex shedding is confirmed for speeds of 10, 20, and 30m/s test cases. The data indicates lower C_P magnitudes for the higher speeds, which was confirmed in the test case with no tabs. The elimination of vortex shedding alludes to the trend that drag will be reduced where tabs were implemented.

VI. Conclusion

Testing of a bluff body with and without end plate tabs was performed in the California Polytechnic State University 3x4 ft low speed wind tunnel. The model was shimmed to obtain equivalent magnitudes for negative C_P spikes for the top and bottom of the mode. The test case was performed when the model was at approximately 5° angle of attack, and it was found that the C_P spikes were at approximately -0.46 for the bottom of the model and approximately -0.38 for the top of the model base at a speed of 30 m/s. The C_P spikes were found to be at approximately -0.36 for the bottom of the model and approximately -0.35 for the top of the model base at 20 m/s, and the spikes were at approximately -0.2 for the bottom and approximately -0.22 for the top of the model base at 15 m/s. The strong negative spikes are indicative of vortex shedding at the top and bottom of the base plate without tabs. The C_P values were computed for calibrated tunnel speeds as the test section will have inherently faster flow than at the inlet for a constant tunnel speed due to the growing boundary layer throughout the length of the tunnel. The calculated dynamic pressures for 15, 20, and 30 m/s contained an error of 1.5%, 2.1%, and 1.2% respectively for these speeds. The trends of the differing test speeds were analyzed, and it was found that the negative C_P spikes

were greater for the higher speed test cases. The vortex shedding was stronger for higher speeds, and this confirms a trend that was not seen in previous test cases performed with no tabs on the model.

The base plate of the model was removed, and tabs were implemented for the next series of tests. The model was oriented at 0° angle of attack, and speeds of 10, 20, and 30 m/s were used for testing. It was observed that the model with tabs exhibited indications that the vortex shedding was eliminated and the strong negative C_P spikes were not observed for the model when tabs were used. This confirms the previous tests that showed elimination of vortex shedding at the top and bottom of the base of the model, effectively reducing the drag for the model. The pressure distributions are relatively constant along the span of the base for the model with tabs. Sources of error may be due to flow asymmetry in the wind tunnel as well as asymmetry of the model mounting with respect to the walls of the wind tunnel. Pressure port number 7 for the test case without tabs was observed to be faulty, and it was averaged in order to observe data trends of the spanwise base plate of the model. It was found that port 7 was clogged when further investigated after testing. This clog was noted in Jarred Pinn's thesis, so it was most likely created during the initial manufacture of the model and should be replaced should the model warrant further testing of the spanwise base. Differences in magnitudes of negative spikes were most likely due to the strut mount at the bottom of the model as the top was free of this obstruction.

Acknowledgments

We would like to thank Dr. Jin Tso for his help and guidance throughout the testing process. Scott Sawyer was also a great help when becoming familiar with test procedures of using the Cal Poly wind tunnel. Jarred Pinn provided an excellent thesis to compare obtained test results to, and his accomplishments with testing of the model should be noted.

References

Aero 307 Liveplot Data Analysis. *Aero 307*. California Polytechnic State University. Web. Apr.-May 2012.

Anderson, John D. *Fundamentals of Aerodynamics*. New York: McGraw-Hill, 2005. Print.

Pinn, Jarred M. "Effect of End-plate Tabs on Drag Reduction of a 3D Bluff Body with a Blunt Base." Thesis. California Polytechnic State University, 2012. Print.

Pope, Alan, and William H. Rae. *Low-speed Wind Tunnel Testing.* New York: Wiley, 1984. Print.

"Sally Hansen Diamond Strength Instant Nail Hardener." *Sears*. Web. 04 June 2012. <http://www.sears.com/shc/s/p_10153_12605_01303105000P?prdNo=12>.

Appendix

A. Matlab code used to sort scannivalve results:

```
function [pressave_psid Q CP] = PAULDATA(filename, ports)
%the data will be loaded and the first term dropped out (.dat)
%the first term must be dropped because the software adds an extra "1" that
%is not needed in the data file, so start at the second value and count
%every four values to get each succesive reading...
tunneldata=importdata(filename);
tunneldata=tunneldata(2:end);%drop first "1" in .dat file
for i=1:length(tunneldata)/4 %split the data into 4 cols
    portnum(i)=tunneldata(4*i-1); %take every third value
    press(i)=tunneldata(4*i); %take every fourth value
end
%now put the data into cols of # of scans
for j=1:length(portnum)/ports
    port_sort(j,:)=portnum((ports*j-(ports-1)):ports*j);%cols are pressures
    press_sort(j,:)=press((ports*j-(ports-1)):ports*j);%cols are row #'s
end
%now average the pressures for each col every row
```

```
for k=1:ports
    pressave_psid(k)=mean(press_sort(:,k));%average across all rows
end
%now find the dynamic pressure
Q=pressave_psid(16)-pressave_psid(17);
for l=1:ports-2
    CP(l)=(pressave_psid(l)-pressave_psid(ports))/Q;
end
end
```

B. Matlab code used to prodce C_P plots and results:

```
%data crunch and output plots for tabs testing
clear all
close all
clc
format compact
x=[-1.5 -1.285 -1.070 -.8561 -.6413 -.4265 -.2117 0 .2117 .4265 .6413 .8561
1.070 1.285 1.5];
%test day five 20m/s
[pressave_psid10tabs Q10tabs CP10tabs] = PAULDATA('10_3tabs.dat', 17)
[pressave_psid20tabs Q20tabs CP20tabs] = PAULDATA('20_1tabs.dat', 17)
[pressave_psid30tabs Q30tabs CP30tabs] = PAULDATA('30_1tabs.dat', 17)
% [pressave_psid5_15 Q5_15 CP5_15] = PAULDATA('day5_15_1night.dat', 17)
%average out the bad port
% CP10tabs(7)=(CP10tabs(8)+CP10tabs(6))/2;
% CP20tabs(7)=(CP20tabs(8)+CP20tabs(6))/2;
% CP30tabs(7)=(CP30tabs(8)+CP30tabs(6))/2;
% CP5_15(7)=(CP5_15(8)+CP5_15(6))/2;
figure(1)
hold all
plot(x,CP10tabs,'*-');
title('CP Distribution With Tabs (Spanwise Direction) ')
xlabel('Spanwise Position Z/h')
ylabel('Base Pressure Coefficient CP')
axis([-1.5 1.5 -.7 -.1])
plot(x,CP20tabs,'*-');
plot(x,CP30tabs,'*-');
% plot(x,CP5_15,'*-');
legend('10m/s','20m/s','30m/s')
hold off
%data crunch and output plots for testing
clear all
close all
clc
format compact
x=[-1.5 -1.285 -1.070 -.8561 -.6413 -.4265 -.2117 0 .2117 .4265 .6413 .8561
1.070 1.285 1.5];
%test day five 20m/s
% [pressave_psid5_10 Q5_10 CP5_10] = PAULDATA('day5_10_3night.dat', 17)
[pressave_psid5_20 Q5_20 CP5_20] = PAULDATA('day5_20_1night.dat', 17)
[pressave_psid5_30 Q5_30 CP5_30] = PAULDATA('day5_30_1night.dat', 17)
[pressave_psid5_15 Q5_15 CP5_15] = PAULDATA('day5_15_1night.dat', 17)
%average out the bad port
% CP5_10(7)=(CP5_10(8)+CP5_10(6))/2;
CP5_20(7)=(CP5_20(8)+CP5_20(6))/2;
CP5_30(7)=(CP5_30(8)+CP5_30(6))/2;
CP5_15(7)=(CP5_15(8)+CP5_15(6))/2;
figure(1)
```

```
hold all
% plot(x,CP5_10,'*-');
title('CP Distribution Without Tabs (Spanwise Direction) ')
xlabel('Spanwise Position Z/h')
ylabel('Base Pressure Coefficient CP')
axis([-1.5 1.5 -0.6 -0.2])
plot(x,CP5_15,'*-');
plot(x,CP5_20,'*-');
plot(x,CP5_30,'*-');
legend('15m/s','20m/s','30m/s')
hold off
```

C. Matlab code used to prodce C_P plots and results with calibrated airspeeds:

```
[pressave_psid5_20] = PAULDATAtest('day5_20_1night.dat', 17)
[pressave_psid5_30] = PAULDATAtest('day5_30_1night.dat', 17)
[pressave_psid5_15] = PAULDATAtest('day5_15_1night.dat', 17)
%find calibrated dynamic pressures and use to solve for CP
Q15=-.002-(-.0249);
Q20=-.0029-(-.0395);
Q30=-.0046-(-.08403);
for l=1:15
    CP15(l)=(pressave_psid5_15(l)-(-.0249))/Q15;
    CP20(l)=(pressave_psid5_20(l)-(-.0395))/Q20;
    CP30(l)=(pressave_psid5_30(l)-(-.08403))/Q30;
end
CP20(7)=(CP20(8)+CP20(6))/2;
CP30(7)=(CP30(8)+CP30(6))/2;
CP15(7)=(CP15(8)+CP15(6))/2;
```